



A computational modelling tool for prediction of head reshaping following endoscopic strip craniectomy and helmet therapy for the treatment of scaphocephaly

Lara Deliege^{a,*}, Alessandra Carriero^b, Juling Ong^c, Greg James^c, Owase Jeelani^c, David Dunaway^c, Petronella Stoltz^d, David Hersh^d, Jonathan Martin^d, Kathleen Carroll^e, Megan Chamis^e, Silvia Schievano^a, Markus Bookland^d, Alessandro Borghi^f

^a University College of London, UK

^b City College of New York, USA

^c Great Ormond Street Hospital, UK

^d Connecticut Children's Hospital, USA

^e Hanger Clinic, USA

^f Department of Engineering, Durham University, DH1 3LE, Durham, UK

ARTICLE INFO

Keywords:

Craniosynostosis
Endoscopic strip craniectomy
Helmet therapy
Finite element modelling
Pre-operative planning

ABSTRACT

Background: Endoscopic strip craniectomy followed by helmet therapy (ESCH) is a minimally invasive approach for correcting sagittal craniosynostosis. The treatment involves a patient-specific helmet designed to facilitate lateral growth while constraining sagittal expansion. In this study, finite element modelling was used to predict post-treatment head reshaping, improving our comprehension of the necessary helmet therapy duration.

Method: Six patients (aged 11 weeks to 9 months) who underwent ESCH at Connecticut Children's Hospital were enrolled in this study. Day-1 post-operative 3D scans were used to create skin, skull, and intracranial volume models. Patient-specific helmet models, incorporating areas for growth, were designed based on post-operative imaging. Brain growth was simulated through thermal expansion, and treatments were modelled according to post-operative imaging available. Mechanical testing and finite element modelling were combined to determine patient-specific mechanical properties from bone samples collected from surgery.

Validation compared simulated end-of-treatment skin surfaces with optical scans in terms of shape matching and cranial index estimation.

Results: Comparison between the simulated post-treatment head shape and optical scans showed that on average 97.3 ± 2.1 % of surface data points were within a distance range of -3 to 3 mm. The cranial index was also accurately predicted ($r = 0.91$).

Conclusions: In conclusion, finite element models effectively predicted the ESCH cranial remodeling outcomes up to 8 months postoperatively. This computational tool offers valuable insights to guide and refine helmet treatment duration. This study also incorporated patient-specific material properties, enhancing the accuracy of the modeling approach.

1. Introduction

Craniosynostosis is a congenital deformity involving the premature closure of one or more cranial sutures during infancy and affects 1 in 2500 newborns [1]. The most common form involves premature ossification of the sagittal suture, causing an elongated and narrow head shape (scaphocephaly). Along with cranial misshaping, premature

suture ossification can result in an increase of intracranial pressure [2,3] as the cranium fails to accommodate brain growth, in rare instances leading to severe headaches, vision loss, and seizures [3].

This condition is managed with a range of surgical procedures, including endoscopic strip craniectomy (ESC) followed by helmet therapy (ESCH) – a minimally invasive procedure aimed at releasing the fused cranial plates and remodeling the deformed cranial vault [4].

* Corresponding author. University College London, Gower Street, London, WC1E 6BT, UK.

E-mail address: sejllie@ucl.ac.uk (L. Deliege).

<https://doi.org/10.1016/j.combiomed.2024.108633>

Received 21 December 2023; Received in revised form 10 May 2024; Accepted 18 May 2024

Available online 23 May 2024

0010-4825/© 2024 The Author(s). Published by Elsevier Ltd. This is an open access article under the CC BY license (<http://creativecommons.org/licenses/by/4.0/>).

During ESC, the fused suture is removed to allow for lateral expansion of the skull driven by the child's fast-growing brain, which acts as a very effective internal distractor [5]. Within 3 days post-surgery, patients' 3D cranial measurements are taken using a computer-aided optical scan which are later used to create fitted cranial orthoses [6]. The orthoses are designed to contact all areas of the cranium except where growth is desirable. In the case of sagittal craniosynostosis (SC) patients, the whole forehead and the occiput are constricted to promote expansion of the medial-lateral dimensions of the cranium [6,7]. The Connecticut Children's craniofacial team instructs families keep patients in their helmet for 22 h each day, 7 days a week [8–10]. Moulding helmets are remodeled to account for patient growth in 2-week intervals, as needed. When a patient outgrows an orthosis, new optical scans are acquired, and a new helmet molded. This typically occurs in 3-month intervals.

Due to the reliance of endoscopic surgical correction on brain growth to support distraction of the calvarium, surgical corrections are best performed in the early in life, usually prior to 4 months of age [5,11–13]. However, since this technology has been recently adopted, many unknowns still remain, such as surgical parameters and the optimal orthosis treatment period to achieve the best functional and cosmetic outcome [14,15]. Lack of pediatric skull mechanical property data due to its limited availability also presents difficulties in predicting the impact of ESC and helmet therapy on patients of different ages. Understanding the biomechanics of cranial remodeling could highlight gaps in care as therapeutic variables can't currently be investigated with randomized controlled trials. Indeed, several studies showcase the importance of this knowledge to accurately model the skull and its alteration by corrective devices. This emphasizes the importance of taking into account both complex material behaviour (such as viscoelasticity, which has an important effect on skull reshaping in spring distraction [16]) as well as age and population specific material properties, which have shown to dramatically affect the outcome of numerical modelling prediction [17].

Computational modeling using finite element method (FEM) is a powerful tool that allows for virtual experimentation while staying within the constraints of determined physical boundaries. Although new to predict the outcomes of ESC followed by helmet therapy, FEM has already been used successfully as a pre-operative planning tool in the treatment of sagittal craniosynostosis [16,18] and other craniofacial procedures [17,19,20]. To date, one preliminary study attempted to replicate the biomechanics of the helmet therapy for sagittal patients using a simplified FE approach on a singular patient [21]. In this study, we will expand our analysis to a larger population using patient-specific properties and include the modelling of the moulding helmet. Additionally, a long-term validation was also conducted to enhance the reliability of our findings. Patient-specific modelling allows investigators to replicate individual tissue properties and accounts for differences in morphological characteristics and other external factors. It thus represents a useful tool to understand this complex problem, provide quantitative assessment of surgical outcomes and help with presurgical planning.

This study aims at creating computational models of sagittal craniosynostosis (SC) correction using experimental and in-silico-testing to

predict subsequent cranial remodeling post-ESCH and during helmet therapy. This will provide an important tool for treatment planning and for designing the next generation of orthotic devices.

2. Methods

2.1. Patient population

Six patients who presented with SC to Connecticut Children's Division of Pediatric Neurosurgery were treated with ESC followed by cranial helmet moulding (age at surgery: 4.2 ± 1.9 months [range from 2.5 to 9 months]) and recruited for this study (Table 1). Each patient received pre-operative and post-operative 3D head-scans: at day 1–3 post procedure, after 3 months of treatment with a first helmet and after 2–5 months of treatment with a second helmet. The helmet therapy was analysed for a period of 3–8 months for this population and the helmet change and/or removal dates are reported in Fig. 1. All research was performed in accordance with Institutional guidelines and ethical codes: informed consent was obtained for all imaging data and bone tissue collections from patients' legal guardians. This study protocol was approved by the Great Ormond Street Hospital and Great Ormond Street Institute of Child Health joint Research and Development Office (Ethical approval number: UK REC 15/LO/0386; internal R&D number 20DS33) and the Connecticut Children's institutional review board [IRB# 19-047]. All procedures performed in this study were in accordance with the 1964 Helsinki declaration and its later amendments or comparable ethical standards.







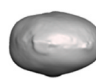



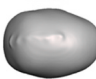
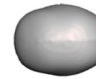
2.2. Surgical technique

Following general anesthesia, each patient was placed in a prone position [22]; sagittal craniectomies were performed through two incisions of approximately 2 cm in length [1] located just posterior to bregma and just anterior to lambda perpendicular to the fused suture [23]. A 1 to 2 cm-wide rectangular craniectomy from the anterior fontanelle to the lambdoid suture, containing the fused suture and some surrounding parietal bone, is then removed using bone scissors [6]. Hemostasis and dural integrity were then verify via direct inspection and valsalvae before closing the incisions. The discarded bone was collected from theatre for the 6 procedures included in this study to allow mechanical testing of the bony tissue.

2.3. Patient-specific cranial bone mechanical properties characterization

Directly after collection, the bone samples were fresh frozen and stored in a -20° freezer. Once defrosted at room temperature, 2-mm wide beams were cut out of these samples in an orientation parallel to the sagittal suture using a diamond bone saw (IsometTM, Buehler, Coventry, UK) under constant irrigation at a suitable distance from the midline such as to avoid any thickening or variations in bone morphology in the test samples (Fig. 2, A). These test samples were kept hydrated by Phosphate buffered saline (PBS) infused gauze until the mechanical testing and were then fixed in 4 % paraformaldehyde (PFA)

Table 1
Patient population analysed in this study with age at surgery.

Patients	P1	P2	P3	P4	P5	P6
						
						
Age at Surgery	3.2 months	9 months	3 months	5 months	4 months	2.5 months

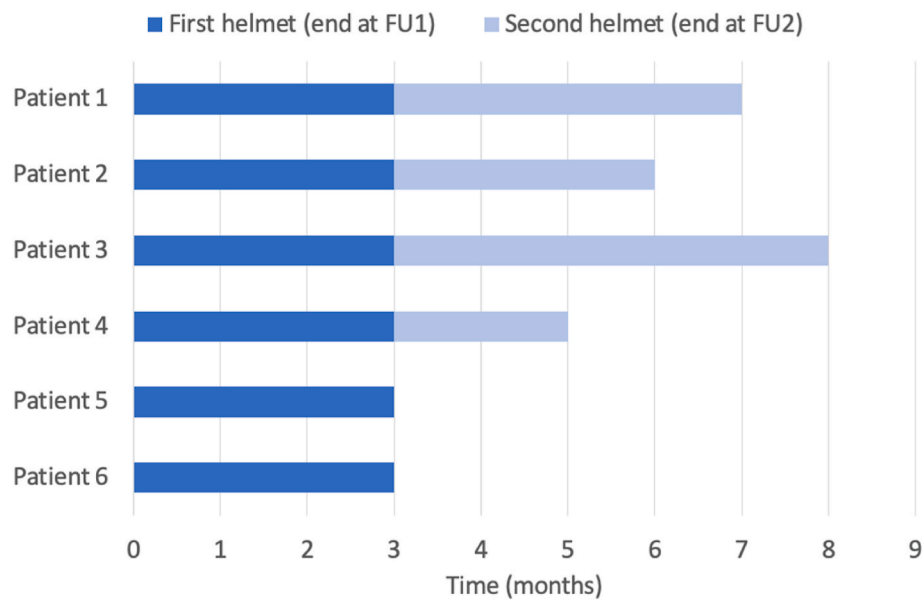


Fig. 1. Treatment timeline for the first and second helmet.

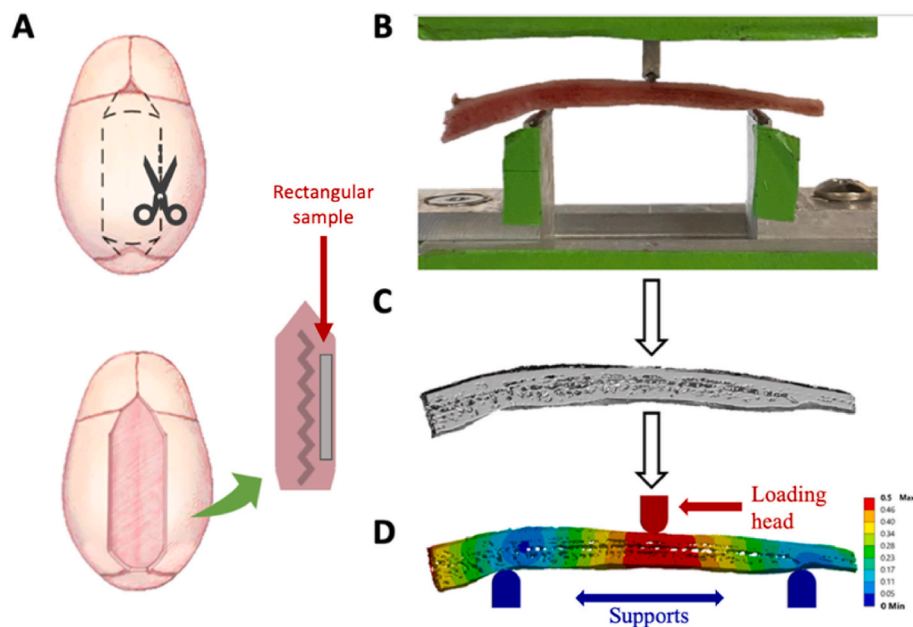


Fig. 2. Outline of sample collection during surgery (A). Modelling framework starting with experimental testing (B) followed by micro-CT scanning (C) and FE modelling (D).

for 24 h before the micro-computed tomography (CT) imaging to stabilize and preserve the morphology and ultrastructure of the biological sample and avoid several freeze-thawing cycles [24].

2.3.1. Mechanical testing

Once cut out to the desired shape, each beam was inserted into a custom three-point bending device for experimental testing (Fig. 2, B). Once positioned, the location of the beams relative to the supports and loading head was visually recorded for further modelling steps.

After applying a pre-load of 0.1 N to secure the beam in place, a bending test was performed on the beams by imposing a displacement of 0.5 mm to the loading head at a rate of 1 $\mu\text{m/s}$. The test was replicated 3 times for each sample and the force-displacement curve, measured using an Interface Inc.® WMC 100 lbf load cell (Berkshire, UK) was recorded.

2.3.2. Micro CT imaging and FE modelling

The 3 point-bending test was later replicated (in terms of testing span, support and indenter curvatures, position of the sample) using Finite element (FE) modelling. The results were then compared with the output of the experimental tests and the material Young's modulus was tuned, in order to extract the sample-specific mechanical properties. This methodology allows the consideration of the beams irregular cross section [25].

After testing, each patient's sample was scanned using a Sky-Scan1172 Bruker micro-CT scanner at a pixel size of 8.93 μm and applying an aluminum filter to reduce artifacts and improve the image quality [26] (50 kV voltage, 201 μA current and approximately 4000 slices per sample). The resulting stack of 2D images was reconstructed using Sky Scan's volumetric NRecon reconstruction software and segmented to isolate the bone tissue in Simpleware ScanIP© (Synopsis,

Mountain View, CA).

Two beam configurations were considered: a porous model (referred here as *Micro-CT model*) extracted directly from the CT reconstruction; a second model obtained in Simpleware ScanIP® by filling in the porous cavities (initially using the *Close* operations and then manually adjusting when necessary) and thus consisted in a solid, non-porous approximation of the beam (referred here as *Solid model*). The porosity (defined as the volume of the pores over the total volume) [27] of each *MicroCT model* was also computed in ScanIP. Spearman correlation was used to assess correlation between patient porosity and age.

Each 3D reconstruction was discretized using linear tetrahedral elements (~2,000,000 elements) and imported in Ansys Mechanical 2020 R2 (Ansys Inc, Canonsburg, Pennsylvania, US) for further analysis (Fig. 2, C).

Both supports and loading head of the three-point bending device were modelled in Solidworks 2021 (Dassault Systems, France) and carefully aligned with the samples to match the position of the sample during the experimental test (Fig. 2, D). The testing span between both supports was chosen as close as possible, following the recommendations outlined by ASTM D790. The assembly of all the in-silico model components was imported in Ansys Mechanical where the supports' bases were fixed in all directions and the same displacement of 0.5 mm was imposed to the loading head, which was assumed to already be in contact at the beginning of the simulation. Contact regions between the beam and both supports were considered frictional, with a friction coefficient of 0.1, while the contact points with the loading head were defined as bonded to avoid rigid movements. For all samples, the material properties of the bone tissue were fixed at 1300 MPa for the reference simulation based on existing literature [25,28] and the simulated force reaction associated to that modulus of elasticity was retained as a parameter. Ansys Design of Experiment (DOE) tool was used to estimate the patient-specific material properties, namely Young's modulus, by comparing simulated and experimentally recorded force-displacement curves. For each patient, two values were extracted: one for the *MicroCT model*, relative to the calvarial bone tissue material properties, and a second for the *Solid Model*, relative to an equivalent non-porous structure having the same bending stiffness. Since the patient-specific skull FE models in this work were considered as solid, homogenous and of constant thickness for simplicity purposes, the *Solid model* was therefore used to provide more appropriate flexural properties of the skull, similarly to other works in the literature [29].

2.4. FE modelling: ESCH followed by helmet therapy

Initial post-operative 3D head scan imaging, obtained using a clinical handheld computer-aided optical scanner (TechMed3D, Quebec, Canada), was utilized to produce the 3D skin models (Fig. 3, A), and the respective skull (Fig. 3, B) and intracranial volume (ICV) (Fig. 3, C) models by means of surface offsetting in Meshmixer®. CAD (computer aided design) models are then created for each component in

Solidworks® where the cranial sutures were mirrored on the skull (Fig. 2, B) along with the creation of the skull base, assumed to lie on the plane passing through nasion and auditory meatuses (Fig. 3, C). A 15 mm-wide osteotomy from cranial bregma to lambda, encapsulating the theoretical fused suture, was modelled on each skull model as per indication of the operating surgeon (Fig. 3, B). Following general pre-operative planning templates (Fig. 4, A), and orthosis clinicians indications, patient-specific fitted helmet models were constructed (Fig. 4, B): starting from a surface in contact with the skin, areas of free space were created using Meshmixer® to allow for growth in targeted areas, using the pre-operative planning template as guide. This helmet model was then halved along the coronal plane (dashed line, Fig. 4 B) to allow a seamless closure around the head.

For each individual patients, all the CAD parts constituting the head (skin, skull, sutures, ICV) and the helmet were assembled and imported in Ansys Workbench (Ansys 2020 R2), a commercial finite element software. The classical linear elastic formulation is considered (Ansys 2022R2 user manual and Slaughter, 2002 [30]), where $\sigma = C : \epsilon$ (with σ the Cauchy stress tensor and C is the stress-strain material tensor), ϵ is the infinitesimal strain tensor - which is related to the displacement vector U by the equation $\epsilon = (\nabla U + \nabla U^T)/2$ - and equilibrium is given by the Cauchy momentum equation $\nabla \cdot \sigma + F = 0$ (where F is body force per unit volume). According to the principle of virtual displacement, for any compatible small virtual displacement acting on a body, the total internal virtual work is equal to the total external work:

$$\int_V \epsilon_V^T \sigma dV = \int_V U_V^T F dV \quad (1)$$

where U_V is the virtual displacement and ϵ_V is the corresponding virtual strain. By approximating the body as an assemblage of finite elements interconnected at nodal points, with displacement $U = H \cdot \hat{U}$ (with H elemental displacement interpolation matrix and \hat{U} nodal displacement vector), element strains can be evaluated as $\epsilon = B \cdot \hat{U}$ (where B is the strain displacement matrix). By summing on the volume of each finite element, equation (1) can be rewritten as

$$\hat{U}^T \cdot \sum \int_V B^T C B dV \cdot \hat{U} = \hat{U}^T \int_V H^T F dV \quad (2)$$

Which can be simplified as

$$K \hat{U} = R \quad (3)$$

where $K = \sum \int_V B^T C B dV$ is structure stiffness matrix and $R = \int_V H^T F dV$ is the equivalent nodal load vector [31]. Calculation of the matrix K and the load vector R allow for solution of equation (3) providing nodal displacement.

The entire model was meshed using linear tetrahedral elements ($432,575 \pm 86,043$ elements). Contact regions between the ICV and the skull as well as the skull and the skin were automatically detected and

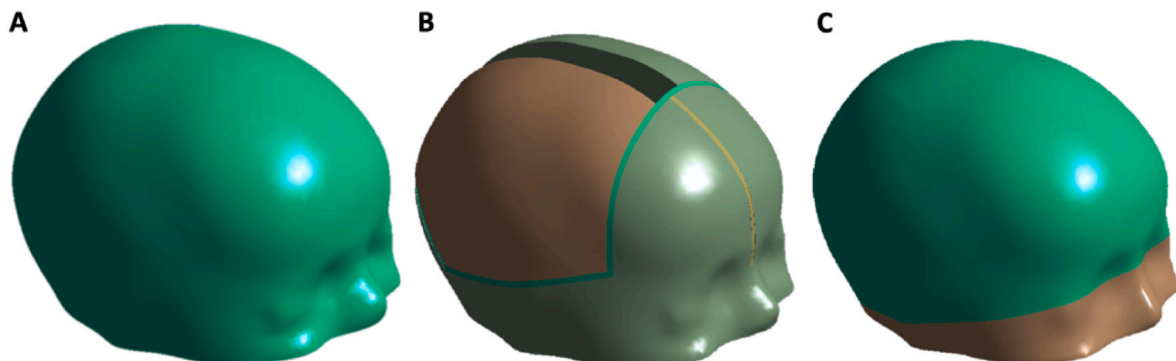


Fig. 3. (A) skin layer created by offsetting the optical scan surface, (B) skull layer with sutures and osteotomy, (C) ICV and skull base.

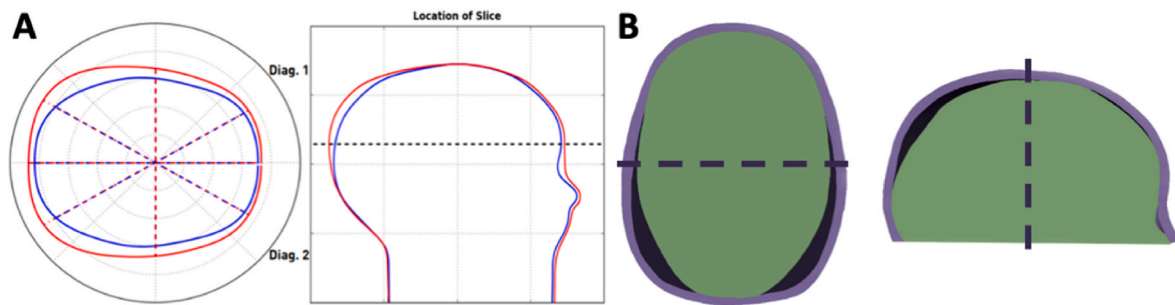


Fig. 4. Template example provided by the orthotic clinic (A) and helmet created for one patient (B).

considered bonded while a frictional contact region was manually defined between the skin and the helmet with a friction coefficient of 0.1. Boundary conditions were defined systematically, fixing the bottom face of the skull base in all directions to mimic tethering of the rest of the head. Simulations for the whole population were divided into 3 loading steps: 1) the front part of helmet was translated and fitted around the head; 2) the back part was displaced in the same way, to simulate helmet closure; 3) the head growth was modelled using an isotropic thermal expansion model of the ICV implemented in ANSYS which was proposed and validated by Libby et al. [32].

$$\Delta V = V_1 \times \alpha \times \Delta T \quad (4)$$

Where α is the coefficient of thermal expansion, ΔT is a temperature difference arbitrarily fixed at 100 °C (increases during the simulation to trigger the expansion), V_1 is the initial ICV, and ΔV the ICV increase due to growth. The value of α was calibrated and fixed at 0.0006 1/°C for a 3 month-growth based on trial & error testing on a sample patient for which monthly follow-up scans were taken to record the growth as accurately as possible. The helmet was positioned around the head by applying a fixed displacement to the helmet border (both bottom and mid-section).

For each patient, growth was initially simulated for three months for a first helmet model. The resulting deformed shape was then extracted and processed in Meshmixer, to close the osteotomy gap (assumed to be filled with bone by the end of the third month post-op). A second helmet fitting (using the same method and parameter as the first one) was simulated for an additional 2–5 months according to the end of treatment date for each patient.

Patient-specific head models were simulated using patient-specific linear elastic material properties for the skull (previously extracted using the FE modelling of the samples' bending tests) while linear elastic properties from literature were used for the skin ($E_{\text{skin}} = 1$ MPa [33]), sutures ($E_{\text{sutures}} = 16$ MPa [16]), and ICV ($E_{\text{ICV}} = 100$ MPa [32]). Cranial helmets are fabricated using 12 mm-thick Surlyn plastic (modelled as linear elastic material, $E_{\text{Surlyn}} = 2$ GPa, *Curbell Plastics*).

Intermediate and end-of-treatment shape predictions were validated by comparing with post-treatment optical scans. The two surfaces were aligned and cut along the plane passing through nasion and auditory meatuses to discard the face; both surfaces were then imported in Simpleware ScanIP® to generate the surface deviation. The percentage of surface points within the [-3; +3]mm interval, usually considered in maxillofacial surgery planning [34], was assessed. Pressure values observed between the skin and the helmet were also recorded. The Cranial index (CI) defined as the ratio of head width and the head length, calculated for each predicted head shape was compared to pre-operative values from clinical notes.

3. Results

3.1. Mechanical properties

On average, the 6 beams collected were approximately 49 mm in length, 2.2 mm in width and 2.1 mm in thickness. Results of the three-point bending test FE models were analysed and the elastic modulus for each sample was estimated twice, once simulating deflection on the beam model extracted from the MicroCT images, (E_{MicroCT}), once repeating the same simulation but assuming solid beam configuration (E_{Solid}). The elastic moduli corresponding to the MicroCT bone model was 1761.2 ± 819.2 MPa while for the solid model was 1173.2 ± 596.2 MPa. Table 2 summarizes all the results. Samples porosity was calculated in Simpleware and possible correlation with the age was suggested by spearman correlation test ($r = -0.77$, $p = 0.053$).

3.2. Validation FE modelling at the end of treatment

The orthosis treatment was simulated over 3 months ($n = 2$) or over 5–8 months ($n = 4$). Surface deviations between the simulated post-treatment head shape and the relative post-operative optical scans are shown in Fig. 5. Results showed that $97.3\% \pm 2.1\%$ of the FE simulated surface points were located within an interval of deviation of [-3; +3] mm from the post-operative optical scan surface. Maximal growth (i.e., deformation) for each patient was measured at the removal of the last helmet by adding the total Euclidean displacements reached in Ansys Mechanical at the end of both helmet treatments (Table 3).

The pre-operative and post-treatment CI measurements retrieved from clinical notes were used for the comparison with the simulated FE model. The average end-of-treatment cranial index (CI) recorded was 77.4 ± 2.7 and the simulated FE model yielded similar values with an average of 77.0 ± 2.6 . A comparison of both CIs can be found in Table 4 for each patient, showing good correlation ($r = 0.91$), with no bias. Pressure values recorded between the skin and the helmet displayed in Fig. 6 show a consistent pressure pattern at the end of treatment with the first orthosis i.e., after the first 3 months of correction.

4. Discussion

In this work, a computational modelling approach was adopted to

Table 2
Porosity and Elastic modulus values for both MicroCT and solid-approximated models proper to each patient.

Samples	Age (days)	Porosity (%)	Micro-CT simulation E_{MicroCT} (MPa)	Solid approximation E_{Solid} (MPa)
6	77	31.8	1238	765
3	91	32.4	894	386
1	98	32.0	3125	1413
5	112	16.2	1950	1418
4	140	27.5	1221	971
2	252	1.7	2139	2086

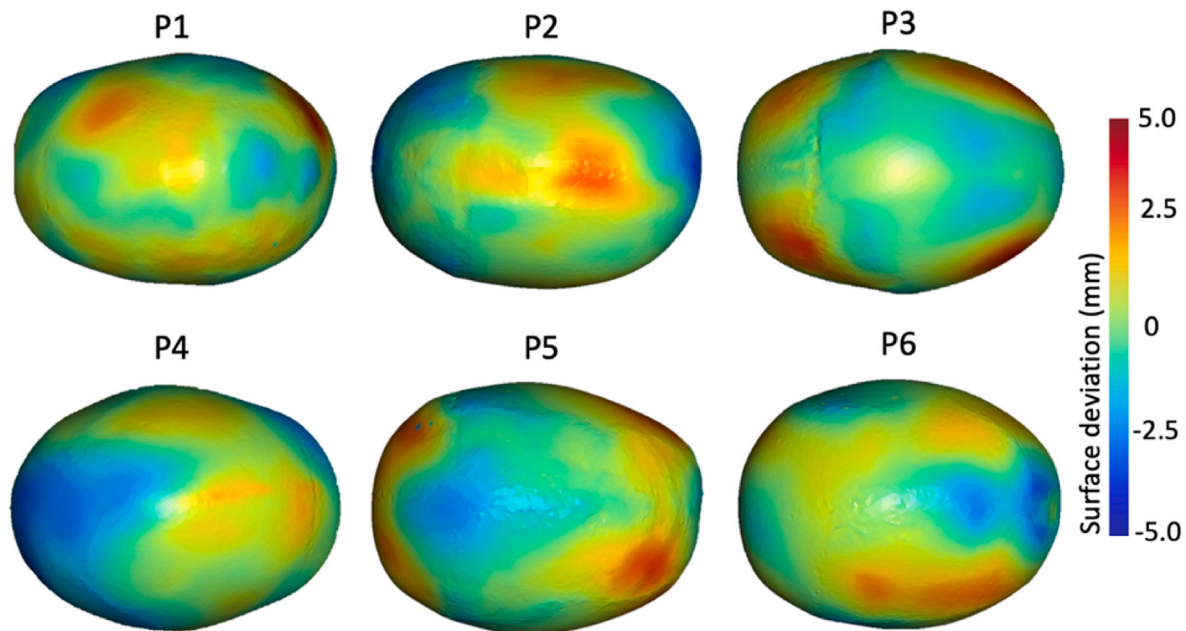


Fig. 5. Surface deviation between the FE prediction and the end-of-treatment optical scans.

Table 3

Total deformation at the end of treatment respective to each patient.

Patient	Treatment time (months)	Total deformation (mm)
1	7	15.8
2	6	11.8
3	8	17.8
4	5	7.3
5	3	5.2
6	3	6.1

Table 4

Quantitative data of all cranial index for all patients at the pre-operative time point as well as end-of-treatment for both the optical scan and simulated model.

Patient	Pre-operative CI (%)	End-of-treatment optical scan CI (%)	End-of-treatment simulated model CI (%)	Prediction error (%)
1	69.5	74.4	74.6	0.2
2	70.0	73.1	72.9	0.2
3	71.2	78.1	76.2	1.9
4	75.8	78.8	79.6	0.8
5	72.7	79.2	79.7	0.5
6	74.2	80.8	78.7	2.1

predict the outcome of endoscopic strip craniectomy followed by helmet therapy in children affected by scaphocephaly caused by sagittal craniosynostosis. The developed FE model was tested on 6 patients who underwent surgery and cranial moulding treatment. This model includes patient-specific 3D geometries i.e., optical head scans, and patient-specific bone material properties. Although simplified geometries were used to create the full head models, good shape matching results were achieved between the numerical results and the patients' end-of-treatment optical scans. Moreover, this study provided insight into the mechanical characteristics of non-syndromic pediatric skulls and built upon a limited existing data in the literature on this subject [29].

To date, only one similar work in the literature [21] investigates the impact of alternating duration of helmet therapy on one skull morphology using FE modelling; however, nodal constraints were applied to model the effect of the helmet rather than an actual helmet geometry. The authors report the pressure exercised on the brain during

different treatment durations: similar pressure values were observed in this study despite the geometric simplifications; therefore we can conclude that our results are consistent with those already published. Cross et al.'s work [21] concentrates on a sample patient geometry (who did not undergo ESCH) and therefore their results may not be generalizable. The absence of validation further highlights the need for cautious interpretation when considering the implications of the paper. Special attention in the present work was paid to patient-specific validation using follow-up images, to ensure our model successfully replicates the progression of the orthotic therapy in-vivo.

Furthermore, the inclusion of a full helmet model allows the quantification of contact pressure between the skin and the helmet. In the present model, foam padding (which is usually included to help distribute loads) was not included and the resulting values may be higher than reality; however the results presented provide patient specific pressure patterns which could be used to predict high pressure areas during calvarial growth. Such information could prove useful screening for at-risk regions for skin injury or ensuring that orthotic designs adequately account for regions of undesirable regions of post-surgical growth. Ongoing work will be looking into the impact of a layer of foam lining the inside of the helmet to further understand the pressure repartition to optimize the esthetic outcomes while minimizing pressure points. The introduction of this preliminary computational model for ESCH, may serve as a tool to refine and improve the surgical management of craniosynostosis. By leveraging computational simulations, this innovative method enables personalized and precise treatment planning, refining surgical procedures and allowing for tailored orthotic treatments. By understanding the mechanical forces at work that remoulds the infant head into a normocephalic volume, surgeons and orthotists may identify redundant osteotomies, orthosis contact points, and moulding durations that could be modified—improving clinical outcomes, simplifying treatment courses, and reducing costs.

In this study, patient-specific material properties were obtained using the FE modelling of the three-point bending test by joining micro-CT imaging to information collected during the experiment. Overall, the resulting Young's Modulus for our MicroCT and solid-approximated samples showed to be in line with previously reported values in the literature (Fig. 7). Comparing studies containing samples within the age range of this study (2.5–9 months), we found that the values reported in this work were generally smaller than the values obtained by Igo et al.

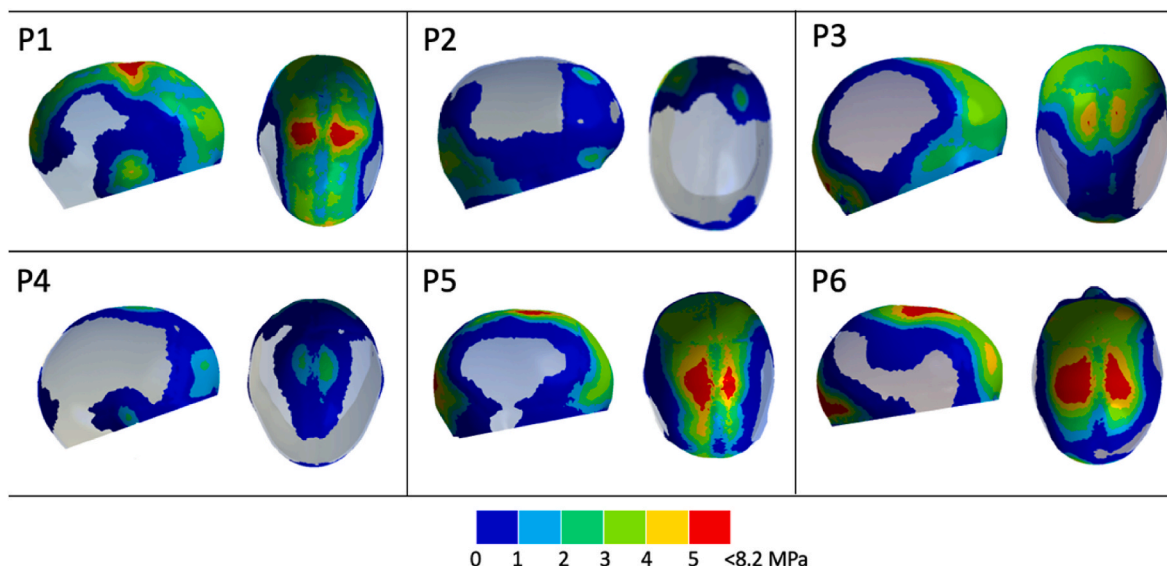


Fig. 6. Pressure patterns after 3 months i.e., at the end of treatment with the first orthosis.

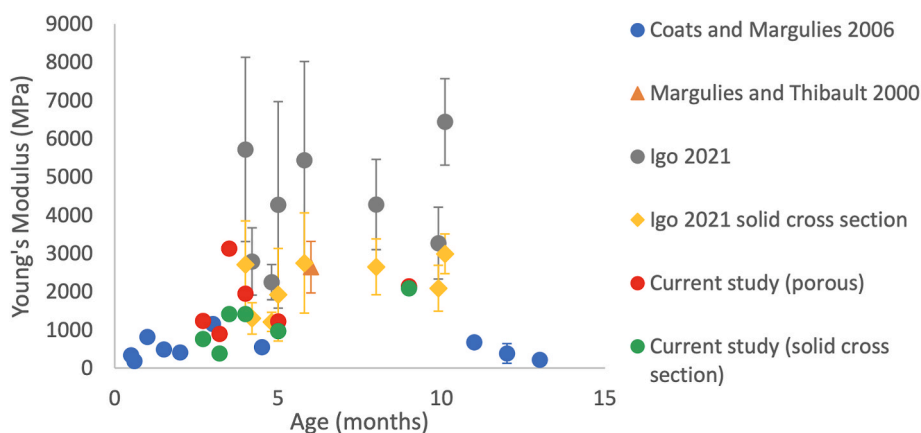


Fig. 7. Comparison of pediatric parietal bone elastic moduli from this and prior studies until 15 months of age.

(2021) [29] using never-frozen porous bone from craniosynostosis patients, but values were closer when compared to their solid-approximated cross-section samples. Values observed by Margulies and Thibault (2000) [35] using fresh-frozen bone (with no cranial deformities) were found to be similar to our findings. For the younger fraction of our cohort (2.5–5 months), our results also agree with the values determined by Coats and Margulies (2006) [36]. All the samples tested were extracted from the parietal bone parallel to the sagittal suture, similarly to Igo et al. [29] and the other studies. Coats and Margulies (2006) also tested occipital bone which showed greater elastic moduli, but these weren't included in this comparison.

For prospective use, the preliminary population curve can be used to match the average elastic modulus to the patient's age. It, however, must be noted that the analysis resulting from the FE modelling didn't acknowledge the different bone morphologies i.e., unilaminar and trilaminar. A previous study from Ajami et al. [25], highlighted that bone structure also influence its bending stiffness. This categorization will be explored in future evaluations.

5. Limitations

A limited number of patients were selected for this pilot study. Future investigations informed by this study will expand this cohort, but these exploratory results must be weighted by the small sample size.

In this work, helmet models were retrospectively recreated based on patient-specific templates of sagittal synostosis patients provided by the orthotic clinic as well as follow-up optical scans of the patient group analysed and the guidance of the operating surgeons. Orthotic helmets are tailored for each patient's needs but will generally always restrict the anterior-posterior movement to promote lateral and vertex growth. Future work will ensure full 3D models of the helmets employed in the therapy will be replicated in the simulations.

The results show that 97.3 % ± 2.1 % of the predicted mode surface points were located within an interval of deviation of [-3; +3] mm from the post-operative optical scan surface. It is worth noting that the peak absolute error was in the range of [3.9; 5.1] mm for the overall population. Patient 5 showed the most significant deviation error, achieving a 94 % match with the corresponding post-operative scan. However, this patient only had one follow-up scan after 3 months of treatment with a first helmet available. This error could therefore be explained by the fact that the FE model might not accurately track the changes in the earliest stages of remodeling compared to the long-term effect. It is possible that the growth is non-linear, suggesting the need for a non-linear growth model to accurately account for this variation. Future work will investigate and implement such a model to better understand and predict the growth dynamics.

The evolution of facial features wasn't included in the present work and the simplified anatomy and boundary conditions implied no facial

growth was allowed in the model. Therefore, validation was also limited to the calvarial section of the head above the nation/tragions plane. Works in the literature [37,38] have analysed skull growth in the pediatric population and showed different growth patterns in the calvarium and mid-face, therefore such level of complexity should be taken into account in future studies.

6. Conclusions

In conclusion, this numerical modelling approach for predicting outcomes of endoscopic strip craniectomy followed by helmet therapy in children affected by sagittal craniosynostosis demonstrates promising results. Despite a limited patient pool, the model incorporated patient-specific properties and achieved satisfactory shape matching. The inclusion of a full helmet geometry in our modelling allowed for the assessment of contact pressure distribution, offering possibilities in addressing skin issues. Ongoing research explores further optimizations, including the use of foam lining in helmets and the application to other types of synostoses i.e., unicoronal, metopic or non-synostotic head deformation, such as positional plagiocephaly.

Summary

Craniosynostosis, a congenital deformity involving premature cranial suture closure, affects 1 in 2500 newborns. The most common type, sagittal craniosynostosis (SC), is managed with endoscopic strip craniectomy (ESC) and subsequent helmet therapy (ESCH). ESC involves removing the fused suture, allowing lateral skull expansion driven by the growing brain. Helmets, designed from post-operative 3D scans, restrict growth in specific areas, promoting overall cranial reshaping. However, uncertainties persist regarding optimal treatment parameters.

This study addresses these gaps through a comprehensive approach, integrating experimental and computational methods. Six patients (11 weeks–9 months old) who underwent ESCH at Connecticut Children's Hospital were enrolled. Patient-specific helmet models, incorporating growth areas, were designed based on post-operative imaging. Finite element modeling simulated brain growth through thermal expansion, and mechanical testing determined patient-specific bone properties. Validation compared simulated post-treatment head shapes with optical scans, demonstrating 97.3 ± 2.1 % accuracy within a -3 to 3 mm distance range. The cranial index was also accurately predicted ($r = 0.91$).

Finite element models effectively predicted ESCH cranial remodeling outcomes up to 8 months postoperatively, providing valuable insights into treatment duration. This computational tool, incorporating patient-specific material properties, enhances modeling accuracy. The study contributes to understanding the biomechanics of cranial remodeling, optimizing surgical and orthotic interventions for SC. The findings guide and refine helmet treatment duration, ultimately improving functional and cosmetic outcomes for affected individuals.

CRedit authorship contribution statement

Lara Deliege: Writing – review & editing, Writing – original draft, Visualization, Validation, Methodology. **Alessandra Carriero:** Writing – review & editing, Methodology. **Juling Ong:** Writing – review & editing. **Greg James:** Writing – review & editing. **Owase Jeelani:** Writing – review & editing, Resources, Project administration. **David Dunaway:** Writing – review & editing, Resources, Project administration. **Petronella Stoltz:** Writing – review & editing. **David Hersh:** Writing – review & editing. **Jonathan Martin:** Writing – review & editing. **Kathleen Carroll:** Writing – review & editing. **Megan Chamis:** Writing – review & editing. **Silvia Schievano:** Writing – review & editing, Resources, Project administration, Conceptualization. **Markus Bookland:** Writing – review & editing, Writing – original draft, Supervision, Methodology, Conceptualization. **Alessandro Borghi:** Writing – review & editing, Writing – original draft, Supervision, Project

administration, Methodology, Conceptualization.

Declaration of competing interest

None to declare.

Acknowledgements

The work has been funded by Great Ormond Street Hospital for Children Charity (grant number 12SG15) as well as the NIHR Biomedical Research Centre Advanced Therapies for Structural Malformations and Tissue Damage pump-prime funding call (grant n. 17DS18), the Great Ormond Street Hospital Charity Clinical Research Starter Grant (grant n. 17DD46), the European Research Council (ERC-2017-StG-757923) and the Royal Society (research grant RGS/R1\231233). This report incorporates independent research from the National Institute for Health Research Biomedical Research Centre Funding Scheme. The views expressed in this publication are those of the author(s) and not necessarily those of the NHS, the National Institute for Health Research or the Department of Health.

References

- [1] M.R. Proctor, Endoscopic craniosynostosis repair, *Transl. Pediatr.* 3 (3) (2014) 247–258, <https://doi.org/10.3978/j.issn.2224-4336.2014.07.03>.
- [2] G. Tamburrini, M. Caldarelli, L. Massimi, P. Santini, C. Di Rocco, Intracranial pressure monitoring in children with single suture and complex craniosynostosis: a review, *Child's Nerv. Syst.* 21 (10) (Oct. 2005) 913–921, <https://doi.org/10.1007/s00381-004-1117-x>.
- [3] P.K. Eide, E. Helseth, B. Due-Tønnessen, T. Lundar, Assessment of continuous intracranial pressure recordings in childhood craniosynostosis, *Pediatr. Neurosurg.* 37 (6) (2002) 310–320, <https://doi.org/10.1159/000066311>.
- [4] C.M. Rudolph, A.N. Awad, K. Toth, M.A. Adamo, C. Carpenter, Endoscopic strip craniectomy and helmet therapy for sagittal craniosynostosis: an analysis of cranial growth changes in the early postoperative period, *Cleft Palate-Craniofacial J.* (105566562211311) (Oct. 2022), <https://doi.org/10.1177/10556656221131119>.
- [5] H.H.K. Delye, W.A. Borstlap, E.J. van Lindert, Endoscopy-assisted craniosynostosis surgery followed by helmet therapy, *Surg. Neurol. Int.* 9 (1) (2018) 59, https://doi.org/10.4103/sni.sni.17_18.
- [6] N.K. Leclair, et al., Rate of craniometric change following suture release in patients with metopic and sagittal craniosynostosis, in: *Journal Of Neurosurgery: Pediatrics*, American Association of Neurological Surgeons, Oct. 2022, pp. 66–73, <https://doi.org/10.3171/2021.7.PEDS21239>.
- [7] D.C. Nguyen, et al., One hundred consecutive endoscopic repairs of sagittal craniosynostosis: an evolution in care, *J. Neurosurg. Pediatr.* 20 (5) (Oct. 2017) 410–418, <https://doi.org/10.3171/2017.5.PEDS16674>.
- [8] R.M. van Wijk, L.A. van Vlimmeren, C.G.M. Groothuis-Oudshoorn, C.P.B. Van der Ploeg, M.J. IJzerman, M.M. Boere-Boonekamp, Helmet therapy in infants with positional skull deformation: randomised controlled trial, *BMJ* 348 (may01 8) (May 2014), <https://doi.org/10.1136/bmj.g2741> g2741–g2741.
- [9] M. Seruya, A.K. Oh, J.H. Taylor, T.M. Sauerhammer, G.F. Rogers, Helmet treatment of deformational plagiocephaly, *Plast. Reconstr. Surg.* 131 (1) (Jan. 2013) 55e–61e, <https://doi.org/10.1097/PRS.0b013e3182729f11>.
- [10] H.-S. Yoo, D.K. Rah, Y.O. Kim, Outcome analysis of cranial molding therapy in nonsynostotic plagiocephaly, *Arch Plast Surg* 39 (4) (Jul. 2012) 338–344, <https://doi.org/10.5999/aps.2012.39.4.338>.
- [11] R.K. Wong, J.K. Emelin, H.S. Meltzer, M.L. Levy, S.R. Cohen, Nonsyndromic craniosynostosis, *J. Craniofac. Surg.* 23 (7) (Oct. 2012) S119–S123, <https://doi.org/10.1097/SCS.0b013e318271cdd2>.
- [12] D.F. Jimenez, C.M. Barone, Endoscopic craniectomy for early surgical correction of sagittal craniosynostosis, *J. Neurosurg.* 88 (1) (Oct. 1998) 77–81, <https://doi.org/10.3171/jns.1998.88.1.0077>.
- [13] A. Mohanty, T.S. Frank, S. Mohamed, K. Godwin, G.G. Malkani, Ultra-early synostectomy and cranial remodeling orthoses in the management of craniosynostoses, *Neurosurg. Focus* 50 (4) (Oct. 2021) E8, <https://doi.org/10.3171/2021.1.FOCUS201014>.
- [14] R.R. Iyer, X. Ye, Q. Jin, Y. Lu, L. Liyanage, E.S. Ahn, Optimal duration of postoperative helmet therapy following endoscopic strip craniectomy for sagittal craniosynostosis, *J. Neurosurg. Pediatr.* 22 (6) (Oct. 2018) 610–615, <https://doi.org/10.3171/2018.5.PEDS184>.
- [15] J.T. Goodrich, Single incision endoscope-assisted surgery for sagittal craniosynostosis, *Child's Nerv. Syst.* 33 (1) (Oct. 2017) 7–8, <https://doi.org/10.1007/s00381-016-3229-5>.
- [16] A. Borghi, et al., A population-specific material model for sagittal craniosynostosis to predict surgical shape outcomes, *Biomech. Model. Mechanobiol.* 19 (4) (Oct. 2020) 1319–1329, <https://doi.org/10.1007/s10237-019-01229-y>.
- [17] L. Deliege, et al., Validation of an in-silico modelling platform for outcome prediction in spring assisted posterior vault expansion, *Clin. BioMech.* 88 (Oct. 2021), <https://doi.org/10.1016/j.clinbiomech.2021.105424>.

- [18] A. Borghi, et al., Spring assisted cranioplasty: a patient specific computational model, *Med. Eng. Phys.* 53 (Oct. 2018) 58–65, <https://doi.org/10.1016/j.medengphy.2018.01.001>.
- [19] C. Cross, et al., Using sensitivity analysis to develop a validated computational model of post-operative calvarial growth in sagittal craniosynostosis, *Front. Cell Dev. Biol.* 9 (May 2021), <https://doi.org/10.3389/fcell.2021.621249>.
- [20] S. Bozkurt, A. Borghi, L.S. van de Lande, N.U.O. Jeelani, D.J. Dunaway, S. Schievano, Computational modelling of patient specific spring assisted lambdoid craniosynostosis correction, *Sci. Rep.* 10 (1) (Dec. 2020), <https://doi.org/10.1038/s41598-020-75747-6>.
- [21] C. Cross, H. Delye, R.H. Khonsari, M. Moazen, A preliminary analysis of replicating the biomechanics of helmet therapy for sagittal craniosynostosis, *Child's Nerv. Syst.* 39 (4) (Oct. 2023) 989–996, <https://doi.org/10.1007/s00381-022-05792-1>.
- [22] Z. Taheri, T. Babae, E. Moradi, B. Hajiaghahi, H.R. Mohammadi, Minimally invasive craniectomy and postoperative cranial remodeling orthotic treatment in infants with craniosynostosis: a multicenter prospective study, *World Neurosurg.* 19 (Oct. 2023) 100207, <https://doi.org/10.1016/j.wnsx.2023.100207>.
- [23] K.L. Chaichana, G.I. Jallo, A.H. Dorafshar, E.S. Ahn, Novel use of an ultrasonic bone-cutting device for endoscopic-assisted craniosynostosis surgery, *Child's Nerv. Syst.* 29 (7) (Oct. 2013) 1163–1168, <https://doi.org/10.1007/s00381-013-2043-6>.
- [24] N. Peredo, R. Valle-Tenney, S. Melis, M. Mesnieres, E. Nefyodova, C. Maes, Visualization and quantification of the stromal-vascular compartment in fetal or adult mouse bones: from sampling to high-resolution 3D image analysis, *STAR Protoc.* 3 (1) (Oct. 2022) 101222, <https://doi.org/10.1016/j.xpro.2022.101222>.
- [25] S. Ajami, et al., Mechanical and morphological properties of parietal bone in patients with sagittal craniosynostosis, *J. Mech. Behav. Biomed. Mater.* 125 (Oct. 2022), <https://doi.org/10.1016/j.jmbbm.2021.104929>.
- [26] M.R. Mani, A.M. Christensen, A. Rafiq, Effects of water and other filters on fracture resolution in industrial micro-CT scanning, *Forensic Imaging* 37 (Jun. 2024) 200588, <https://doi.org/10.1016/j.fri.2024.200588>.
- [27] M.L. Bouxsein, S.K. Boyd, B.A. Christiansen, R.E. Guldborg, K.J. Jepsen, R. Müller, Guidelines for assessment of bone microstructure in rodents using micro-computed tomography, *J. Bone Miner. Res.* 25 (7) (Jul. 2010) 1468–1486, <https://doi.org/10.1002/jbmr.141>.
- [28] J. Wang, et al., Mechanical properties of cranial bones and sutures in 1–2-year-old infants, *Med. Sci. Mon. Int. Med. J. Exp. Clin. Res.* 20 (Oct. 2014) 1808–1813, <https://doi.org/10.12659/MSM.892278>.
- [29] B.J. Igo, P.S. Cottler, J.S. Black, M.B. Panzer, The mechanical and microstructural properties of the pediatric skull, *J. Mech. Behav. Biomed. Mater.* 120 (Aug. 2021) 104578, <https://doi.org/10.1016/j.jmbbm.2021.104578>.
- [30] W.S. Slaughter, *The Linearized Theory of Elasticity*, Springer Science & Business Media, 2002.
- [31] K.-J. Bathe, *Formulation of the finite element method*, in: H. Prentice (Ed.), *Finite Element Procedures*, second ed., Pearson Education, Inc., 2006, pp. 148–338.
- [32] J. Libby, A. Marghoub, D. Johnson, R.H. Khonsari, M.J. Fagan, M. Moazen, Modelling human skull growth: a validated computational model, *J. R. Soc. Interface* 14 (130) (2017) 20170202, <https://doi.org/10.1098/rsif.2017.0202>.
- [33] P.G.M. Knoops, et al., A novel soft tissue prediction methodology for orthognathic surgery based on probabilistic finite element modelling, *PLoS One* 13 (5) (Oct. 2018) e0197209, <https://doi.org/10.1371/journal.pone.0197209>.
- [34] S.C. Aung, R.C.K. Ngim, S.T. Lee, Evaluation of the laser scanner as a surface measuring tool and its accuracy compared with direct facial anthropometric measurements, *Br. J. Plast. Surg.* 48 (8) (1995) 551–558, [https://doi.org/10.1016/0007-1226\(95\)90043-8](https://doi.org/10.1016/0007-1226(95)90043-8).
- [35] S.S. Margulies, K.L. Thibault, Infant skull and suture properties: measurements and implications for mechanisms of pediatric brain injury, *J. Biomech. Eng.* 122 (4) (Oct. 2000), <https://doi.org/10.1115/1.1287160>.
- [36] B. Coats, S.S. Margulies, Material properties of human infant skull and suture at high rates, *J. Neurotrauma* 23 (8) (Oct. 2006), <https://doi.org/10.1089/neu.2006.23.1222>.
- [37] E. O' Sullivan, et al., The 3D skull 0–4 years: a validated, generative, statistical shape model, *BoneKEy Rep.* 15 (Dec. 2021) 101154, <https://doi.org/10.1016/j.bonr.2021.101154>.
- [38] C. Liang, et al., Normal human craniofacial growth and development from 0 to 4 years, *Sci. Rep.* 13 (1) (Jun. 2023) 9641, <https://doi.org/10.1038/s41598-023-36646-8>.